algorithms

MDPI

Article

Power Flow Solution in Bipolar DC Networks Considering a Neutral Wire and Unbalanced Loads: A Hyperbolic Approximation

Simón Sepúlveda-García [1,†], Oscar Danilo Montoya [2,3,*,†] and Alejandro Garcés [1,†]

[1] Department of Electric Power Engineering, Universidad Tecnológica de Pereira, Pereira 660003, Colombia
[2] Grupo de Compatibilidad e Interferencia Electromagnética, Facultad de Ingeniería, Universidad Distrital Francisco José de Caldas, Bogotá 110231, Colombia
[3] Laboratorio Inteligente de Energía, Facultad de Ingeniería, Universidad Tecnológica de Bolívar, Cartagena 131001, Colombia
* Correspondence: odmontoyag@udistrital.edu.co
† These authors contributed equally to this work.

Abstract: This paper addresses the problem of the power flow analysis of bipolar direct current (DC) networks considering unbalanced loads and the effect of a neutral wire, which may be solidly grounded or non-grounded. The power flow problem is formulated using the nodal admittance representation of the system and the hyperbolic relations between power loads and voltages in the demand nodes. Using Taylor series expansion with linear terms, a recursive power flow method with quadratic convergence is proposed. The main advantage of the hyperbolic approximation in dealing with power flow problems in DC bipolar networks is that this method can analyze radial and meshed configurations without any modifications to the power flow formula. The numerical results in three test feeders composed of 4, 21, and 85 bus systems show the efficiency of the proposed power flow method. All of the simulations were conducted in MATLAB for a comparison of the proposed approach with the well-established successive approximation method for power flow studies in distribution networks.

Keywords: bipolar DC networks; hyperbolic approximation; recursive power flow formula; quadratic convergence; solidly grounded and non-grounded neutral wire

Citation: Sepúlveda-García, S.; Montoya, O.D.; Garcés, A. Power Flow Solution in Bipolar DC Networks Considering a Neutral Wire and Unbalanced Loads: A Hyperbolic Approximation. *Algorithms* **2021**, *15*, 341. https://doi.org/10.3390/a15100341

Academic Editor: Abdulsalam Yassine

Received: 16 August 2022
Accepted: 19 September 2022
Published: 22 September 2022

1. Introduction

1.1. Motivation

Recently, the interest in direct current distribution networks has increased due to their advantages in terms of efficiency and controllability and the advances in semiconductor technologies [1,2]. In addition, several distributed energy resources, such as storage devices, photovoltaic panels, and loads, operate directly in DC, reducing the presence of power electronics [3–5]. DC networks are a competitive alternative to AC transmission systems at both high and low voltage levels [6]. Systems at high voltage levels are called HVDC systems (i.e., high-voltage DC), and those at low voltage levels are called LVDC systems (i.e., low-voltage DC) [7]. These grids do not require synchronization and pose economic advantages due to their elimination of the adverse effects caused by reactive power requirements in AC networks [8]. Furthermore, it has been reported that DC networks have low power losses and improved voltage profiles [9].

Models, methods, and algorithms for analyzing conventional AC networks must be extended to DC networks [10,11]. Among these methods, the power flow is perhaps the most important, since it is part of every operation, control, or planning model of electric systems. Despite its apparent simplicity, a power flow for DC networks brings challenges, especially for bipolar networks, namely, networks that include positive, negative, and neutral wires [12]. It has been reported that bipolar LVDCs are more efficient and flexible than the most known monopolar structure [13,14]. While most of the current investigations involve dynamic studies from the power electronic perspective [14,15], the static case concerning the power flow has received little attention, and the utility perspective and steady-state analysis have been neglected.

1.2. Brief State of the Art

The power flow is an indispensable method in electrical grids that determines the state variables for a given operation scenario [16]. This method is used for protection design [17] and as part of optimization models, such as the optimal selection of conductors [18], location of distributed generators and batteries [19], and reconfiguration [20], among others. The power flow is also part of operation models, such as the secondary [21,22] and tertiary control [23]. The latter is particularly relevant, since most tertiary controls are based on optimal power algorithms. The difference between the power flow (PF) and optimal power flow (OPF) is that the latter aims to optimize the operation according to a measure of performance, which is known as the objective function, while considering technical constraints. These constraints include the system model represented by the power flow equations [24]. Therefore, the PF is a part of the set of constraints of the OPF.

The specialized literature has proposed a broad type of power flow method for monopolar DC networks; such methods are classified into the derivative-based and derivative-free categories. Successive approximation, the triangular method, and the backward–forward sweep algorithm are examples of derivative-free methods, whereas hyperbolic approximation, product approximation, and the Newton–Raphson methods are examples of derivative-based methods (see [25] for a complete review of these methods). As their names indicate, the main difference between derivative-based and derivative-free methods is the requirement of a Jacobian (i.e., a derivative) of the set of algebraic functions. Derivative-based methods usually have a quadratic convergence inherited from Newton's algorithm, whereas derivative-free methods have linear convergence. Thus, derivative-based methods may converge in a lower number of iterations. However, building the Jacobian and solving the resulting linear systems may be computationally cumbersome; hence, the calculation time may be longer for derivative-based methods [16]. Moreover, some methods are only applicable for radial networks (e.g., the triangular method), while others (most of them derivative-based) are applicable for both radial and meshed grids. These generic power flow methods have only been studied for monopolar DC networks, except for the successive and triangular approximations, which were analyzed in [26], and the Newton–Raphson method, which was analyzed in [27] for bipolar grids. The former proposal only applied to radial systems and required a large number of iterations for convergence. In contrast, the latter proposal was very detailed, including models of loads, droop controls, and voltage controls, making the power flow model non-general and hardly applicable for other studies, such as those of optimal planning, where a simple power flow formulation with constant power loads at its peak magnitude is enough for the analysis.

The major challenge in studying the power flow in bipolar LVDC networks is the power injection model that is commonly used to represent the grid. In [28], the problem was reformulated into a current injection equivalent that considered detailed models of loads and droops controls for distributed generators. It was a derivative-based algorithm that required the inverse of the Jacobian matrix in each iteration. Therefore, it may be computationally demanding for large test systems. In [29], the problem was also formulated as an equivalent current injection mode with a locational marginal price to reduce congestion between the two poles. Meanwhile, in [30], a methodology was proposed to reduce the voltage imbalance by redistributing the load to reduce power losses; this method assumed a grounded neutral wire in all of the nodes, which was a noticeable oversimplification of natural systems. These methodologies focused on the operative problem and can hardly be generalized to cover other studies concerning bipolar LVDC networks. Therefore, it is necessary to analyze a simpler and more general formulation that may be used in other studies, such as planning, reconfiguration, and protection.

1.3. Contributions and the Article's Outline

This article proposes a general model for power flow analysis in a bipolar DC grid. The contributions are twofold:

- A generalized power flow approximation based on the Taylor expansion of the nonlinear relation between currents and voltages, which includes a neutral pole that is either solidly grounded or non-grounded. This approximation could be used for different studies, such as planning and operation, among others.
- A set of numerical experiments in different benchmark test systems confirms that the hyperbolic approximation is applicable for meshed and radial grids, demonstrating the scalability of the model and the low number of iterations, even for large networks.

The remainder of the paper is organized as follows: Section 2 presents the formulation of the power flow in a bipolar LVDC system, and the approximation for the hyperbolic expressions is discussed to obtain a hyperbolic recursive formulation for solving the PF problem. Section 3 presents the test feeders that will be used in the present paper. Section 4 presents the computational validation of the proposed methodology; finally, Section 5 presents the conclusions and future work.

2. Formulation of the Power Flow Problem

2.1. General Representation

A general representation of a bipolar DC network is given in Figure 1. It consists of a grid with a positive pole p, a negative pole n, and a neutral pole o that may be solidly grounded. In a given node k, the bipolar grid could contain multiple loads connected between positive and negative poles $p_{dk,p-n}$ or between positive and neutral poles $p_{dk,po}$ (analogously, a negative and neutral pole $p_{dk,no}$). Naturally, the system may be unbalanced. To deal with multiple constant power loads, we start with the analysis of the solidly grounded case and then extend the formulation to the non-grounded case.

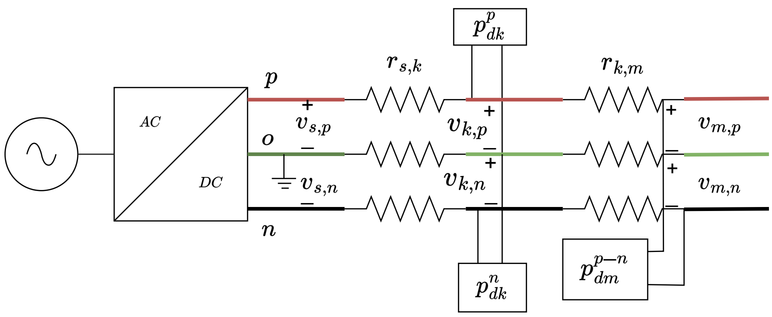

Figure 1. Schematic representation of a bipolar DC network.

The bipolar DC grid is represented by an oriented graph $\mathcal{F} = \{\mathcal{L}, \mathcal{E}\}$, where $\mathcal{L} = \{1, 2, \ldots, l\}$ is the set of hypernodes and $\mathcal{E} \subseteq \mathcal{L} \times \mathcal{L}$ is the set of hyperbranches. Each hypernode and hyperbranch has three components represented by the set $\mathcal{B} = \{p, o, n\}$; these contain the positive, neutral, and negative poles. In this manuscript, the subscripts k and m are entries of $\mathcal{L}$, and the electrical connections are represented by the nodal conductance matrix $\mathbf{G}_{\text{bus}}$. Capital letters represent vector variables or constants, while capital bold letters represent matrix variables or constants, and their entries are lower-case letters. The main variables, constants, and indices are presented in the nomenclature below. In the present work, we call the loads connected between a positive and negative pole a C-type connection, and we call the loads connected between a positive and neutral pole an E-type connection (see Figure 2).

Figure 2. Examples of C-type and E-type loads.

2.2. Solidly Grounded Case

The voltage v_o is zero for solidly grounded systems. Therefore, the general power flow equation for a multinodal bipolar DC can be represented by (1) (in the following equations, h, b, w are entries of the set $\mathcal{B}$):

$$i_{gkE}^{h} - i_{dkE}^{h} - i_{dkC}^{h} = \sum_{b \in \mathcal{B}} \sum_{j \in \mathcal{L}} g_{kj}^{hb} v_k^b, \ \{\forall k \in \mathcal{L}, \ \forall h \in \mathcal{B}\}, \tag{1}$$

where i_{gkE}^{h} is the current generation in the power source connected at node k with an E-type connection in the pole h; i_{dkE}^{h} is the current demanded at node k for a constant-power terminal with an E-type connection in the pole h; i_{dkC}^{h} is the current demanded at node k for a constant-power terminal with a C-type connection in the pole h; g_{kj}^{hb} is the component (entry) of the conductance matrix that relates nodes k and j and the poles h and b, respectively; v_k^b is the voltage at node k for the pole b.

The definitions of the demanded current for the E-type and C-type connections are presented in Equations (2) and (3).

$$i_{dkE}^{h} = \frac{p_{dk}^{h}}{v_k^h}, \tag{2}$$

$$i_{dkC}^{h} = \frac{p_{dk}^{h-w}}{v_k^h - v_k^w}, \tag{3}$$

where p_{dk}^{h} is the power consumed at node k in the pole h with respect to the neutral wire; p_{dk}^{h-w} represents the power consumption at node k between poles h and w. Both (2) and (3) have hyperbolic form.

A linear approximation of (2) and (3) is proposed here. It consists of a Taylor expansion of the hyperbolic representations $f(x) = x^{-1}$ and $g(x, y) = (x - y)^{-1}$ around the operation point (x_0, y_0), which is defined in (4) and (5).

$$f(x) \approx \frac{2}{x_0} - \frac{x}{x_0^2}, \tag{4}$$

$$g(x, y) \approx \frac{2}{x_0 - y_0} - \frac{x - y}{(x_0 - y_0)^2}. \tag{5}$$

Equations (4) and (5) are replaced in (2) and (3), so the equivalent currents for the E-type and C-type connections are found:

$$i_{dkE}^{h} = \left(\frac{2}{v_{k0}^h} - \frac{v_k^h}{\left(v_{k0}^h\right)^2} \right) p_{dk}^{h}, \tag{6}$$

$$i_{dkC}^{h} = \left(\frac{2}{v_{k0}^h - v_{k0}^w} - \frac{v_k^h - v_k^w}{\left(v_{k0}^h - v_{k0}^w\right)^2} \right) p_{dk}^{h-w}. \tag{7}$$

We separate the general power flow Equation (1) into two terms: The first term is related to the slack node, and the second term is associated with the demand nodes. This separation is presented in Equations (8) and (9), respectively.

$$i_{gE}^{pn} = g_{ss}^{pn} v_s^{pn} + g_{sd}^{pn} v_d^{pn}, \tag{8}$$
$$-i_{dE}^{pn} - i_{dC}^{pn} = g_{ds}^{pn} v_s^{pn} + g_{dd}^{pn} v_d^{pn}, \tag{9}$$

where $i_{gE}^{pn} \in \mathbb{R}^{2\times1}$ contains the power injections in the slack node for the positive and negative poles (pn); $i_{dE}^{pn} \in \mathbb{R}^{(2l-2)\times1}$ and $i_{dC}^{pn} \in \mathbb{R}^{(2l-2)\times1}$ are vectors that represent the demanded currents in the E-type and C-type connections. In this definition of the variables, l represents the number of nodes in the bipolar DC grid; $v_s^{pn} \in \mathbb{R}^{2\times1}$ and $v_d^{pn} \in \mathbb{R}^{(2l-2)\times1}$ are vectors that contain the voltage output in the slack node and the voltage variables in the demand nodes for poles pn, respectively; $g_{ss}^{pn} \in \mathbb{R}^{2\times2}$, $g_{sd}^{pn} \in \mathbb{R}^{2\times(2l-2)}$, $g_{sd}^{pn} \in \mathbb{R}^{(2l-2)\times2}$, and $g_{dd}^{pn} \in \mathbb{R}^{(2l-2)\times(2l-2)}$ are submatrices of the general conductance matrix g^{pn}, which relates the slack and demanded nodes.

Equation (8) is linear, since the variables of the power flow problem are the current injections in the slack node, i.e., i_{gE}^{pn}, and the voltages in the demand nodes v_d^{pn}. Hence, its solution is reached when the solution of Equation (9) is found. However, Equation (9) needs to be organized, since vectors with currents i_{dE}^{pn} and i_{dC}^{pn} are dependent of the demanded voltages, as given in (6) and (7).

Let us define the following vectors and matrices:

$$V_d^{pn} = \begin{pmatrix} v_2^p \\ v_2^n \\ \vdots \\ v_L^p \\ v_L^n \end{pmatrix}, \; P_d^{pn} = \begin{pmatrix} P_2^p \\ P_2^n \\ \vdots \\ P_L^p \\ P_L^n \end{pmatrix}, \; P_d^{p-n} = \begin{pmatrix} P_2^{p-n} \\ P_2^{n-p} \\ \vdots \\ P_L^{p-n} \\ P_L^{n-p} \end{pmatrix} \tag{10}$$

$$\mathbf{J} = \begin{pmatrix} 1 & 0 & \dots & 0 & 0 \\ 0 & 1 & \dots & 0 & 0 \\ \vdots & \vdots & \ddots & \vdots & \vdots \\ 0 & 0 & \dots & 1 & 0 \\ 0 & 0 & \dots & 0 & 1 \end{pmatrix}, \; \mathbf{M} = \begin{pmatrix} 0 & 1 & \dots & 0 & 0 \\ 1 & 0 & \dots & 0 & 0 \\ \vdots & \vdots & \ddots & \vdots & \vdots \\ 0 & 0 & \dots & 0 & 1 \\ 0 & 0 & \dots & 1 & 0 \end{pmatrix} \tag{11}$$

where $P_d^{p-n} \in \mathbb{R}^{(2l-2)\times1}$ is the vector of bipolar constant-power loads, $P_d^{pn} \in \mathbb{R}^{(2l-2)\times1}$ is a vector that contains monopolar constant-power terminals, and $\mathbf{J} \in \mathbb{R}^{(2l-2)\times(2l-2)}$ and $\mathbf{M} \in \mathbb{R}^{(2l-2)\times(2l-2)}$ are the identity matrix and an auxiliary matrix that allow the calculation of the voltage differences for bipolar constant-power terminals.

Equations (10) and (11) allow the generalization of the currents in (6) and (7), as presented below:

$$i_{dE}^{pn} = 2\,\mathrm{diag}^{-1}\left(V_d^{pn,t}\right) P_d^{pn} - \mathrm{diag}^{-2}\left(V_d^{pn,t}\right) \mathrm{diag}\left(P_d^{pn}\right) V_d^{pn,t+1} \tag{12}$$

$$i_{dC}^{pn} = \begin{bmatrix} 2\,\mathrm{diag}^{-1}\left((\mathbf{J}-\mathbf{M})V_d^{pn,t}\right) P_d^{pn-np} - \\ \mathrm{diag}^{-2}\left((\mathbf{J}-\mathbf{M})V_d^{pn,t}\right) \mathrm{diag}\left(P_d^{pn-np}\right) (\mathbf{J}-\mathbf{M}) V_d^{pn,t+1} \end{bmatrix} \tag{13}$$

where $\mathbf{V}_d^{pn,t}$ is a linearized vector with the voltage at the iteration t. If Equations (12) and (13) are replaced in Equation (9), then a recursive power flow formula is derived for the bipolar power flow problem with the neutral cable solidly grounded, as presented in Equation (14).

$$\begin{bmatrix} -G_{ds}^{pn} V_s^{pn} - G_{dd}^{pn} V_d^{pn,t+1} + \operatorname{diag}^{-2}\left(V_d^{pn,t}\right) \operatorname{diag}\left(P_d^{pn}\right) V_d^{pn,t+1} + \\ \operatorname{diag}^{-2}\left((\mathbf{J}-\mathbf{M}) V_d^{pn,t}\right) \operatorname{diag}\left(P_d^{pn-np}\right) (\mathbf{J}-\mathbf{M}) V_d^{pn,t+1} - \\ 2\operatorname{diag}^{-1}\left(V_d^{pn,t}\right) P_d^{pn} - 2\operatorname{diag}^{-1}\left((\mathbf{J}-\mathbf{M}) V_d^{pn,t}\right) P_d^{pn-np} \end{bmatrix} = 0 \tag{14}$$

Finally, if we rearrange Equation (14) to obtain a general expression for $V_d^{pn,t+1}$, the following general power flow formula is reached:

$$V_d^{pn,t+1} = -\left[G_{\exp}^{pn}\left(V_d^{pn,t}\right)\right]^{-1} \begin{bmatrix} G_{ds}^{pn} V_s^{pn} + 2\operatorname{diag}^{-1}\left(V_d^{pn,t}\right) P_d^{pn} - \\ 2\operatorname{diag}^{-1}\left((\mathbf{J}-\mathbf{M}) V_d^{pn,t}\right) P_d^{pn-np} \end{bmatrix}, \tag{15}$$

where

$$G_{\exp}^{pn}\left(V_d^{pn,t}\right) = \begin{bmatrix} G_{dd}^{pn} - \operatorname{diag}^{-2}\left(V_d^{pn,t}\right) \operatorname{diag}\left(P_d^{pn}\right) - \\ \operatorname{diag}^{-2}\left((\mathbf{J}-\mathbf{M}) V_d^{pn,t}\right) \operatorname{diag}\left(P_d^{pn-np}\right) (\mathbf{J}-\mathbf{M}) \end{bmatrix}$$

Note that the recursive power flow Formula (15) is evaluated from the initial point $t = 0$ by assigning the voltage at each node that is equal to the substation bus until the convergence criterion is met:

$$\max\left\{\left\| |V_d^{pn,t+1}| - |V_d^{pn,t}| \right\|\right\} \leq \varepsilon, \tag{16}$$

where ε is the acceptable tolerance. Notice that, in this study, the metric for evaluating the convergence process is the voltage variation between iterations; however, some authors make use of the power loss formula as the metric. This requires two additional calculations, the first of which is that of the current across lines and the second of which is that of the power losses in each line; this is less direct than assuming the voltage variation as the metric of convergence [27].

2.3. Non-Grounded Neutral Wire

This subsection explores the extension of the power flow formulation for bipolar DC networks where the neutral wire is uniquely grounded in the substation bus. The main difference in this case is that the current per pole depends on the difference between the pole and load voltages. We define the vector of demanded current per node as i_{dk}^{pon}:

$$i_{dk}^{pon} = \begin{bmatrix} i_{dk}^{p} \\ i_{dk}^{o} \\ i_{dk}^{n} \end{bmatrix} \tag{17}$$

where i_{dk}^{p}, i_{dk}^{o}, and i_{dk}^{n} are the net current injections at node k in the positive, neutral, and negative poles, respectively. These currents are calculated as follows:

$$i_{dk}^{p} = \frac{P_{dk}^{p}}{v_k^p - v_k^o} + \frac{P_{dk}^{p-n}}{v_k^p - v_k^n}, \tag{18}$$

$$i_{dk}^{o} = \frac{P_{dk}^{p}}{v_k^o - v_k^p} + \frac{P_{dk}^{n}}{v_k^o - v_k^n}, \tag{19}$$

$$i_{dk}^{n} = \frac{P_{dk}^{n}}{v_k^n - v_k^o} + \frac{P_{dk}^{n-p}}{v_k^n - v_k^p}, \tag{20}$$

Equations (18)–(20) have the same hyperbolic relation defined for the bipolar current i_{dkC}^{h} in Equation (3). This implies that the currents for the positive, neutral, and negative poles can be approximated as presented in (7) by using the Taylor series expansion with its linear term.

To obtain the power flow formulation for the non-grounded neutral bipolar DC case, we rewrite the matrix Equation (9), as presented in Equation (21).

$$-i_d^{pon} = G_{ds}^{pon} V_s^{pon} + G_{dd}^{pon} V_d^{pon}, \tag{21}$$

where $i_d^{pon} \in \mathbb{R}^{(3l-3)\times 1}$ and $V_d^{pon} \in \mathbb{R}^{(3l-3)\times 1}$ are the vectors of demanded currents and voltages in the demand nodes. $V_s^{pon} \in \mathbb{R}^{3\times 1}$ is the voltage output in the slack node. $G_{ds}^{pon} \in \mathbb{R}^{3\times(3l-3)}$ and $G_{dd}^{pon} \in \mathbb{R}^{(3l-3)\times(3l-3)}$ are submatrices associated with the bipolar conductance matrix considering the neutral wire. To define the general power flow formula for a neutral non-solidly grounded wire, the following vectors are defined.

$$i_d^{pon} = \begin{bmatrix} i_2^p \\ i_2^o \\ i_2^n \\ \vdots \\ i_l^p \\ i_l^o \\ i_l^n \end{bmatrix},\ V_d^{pon} = \begin{bmatrix} v_2^p \\ v_2^o \\ v_2^n \\ \vdots \\ v_l^p \\ v_l^o \\ v_l^n \end{bmatrix},\ P_d^p = \begin{pmatrix} P_2^p \\ P_2^p \\ 0 \\ \vdots \\ P_l^p \\ P_l^p \\ 0 \end{pmatrix},$$

$$P_d^n = \begin{pmatrix} 0 \\ P_2^n \\ P_2^n \\ \vdots \\ 0 \\ P_l^n \\ P_l^n \end{pmatrix},\ P_d^{p-n} = \begin{pmatrix} P_2^{p-n} \\ 0 \\ P_2^{n-p} \\ \vdots \\ P_s^{p-n} \\ 0 \\ P_s^{n-p} \end{pmatrix} \tag{22}$$

in addition, we define the following auxiliary matrices:

$$M_{x_{3\times 3}} = \begin{bmatrix} 1 & -1 & 0 \\ -1 & 1 & 0 \\ 0 & 0 & 1 \end{bmatrix},\ M_{y_{3\times 3}} = \begin{bmatrix} 1 & 0 & 0 \\ 0 & 1 & -1 \\ 0 & -1 & 1 \end{bmatrix},\ M_{z_{3\times 3}} = \begin{bmatrix} 1 & 0 & -1 \\ 1 & 0 & 0 \\ -1 & 0 & 1 \end{bmatrix} \tag{23}$$

matrices $\mathbf{X} \in \mathbb{R}^{(3l-3)\times(3l-3)}$, $\mathbf{Y} \in \mathbb{R}^{(3l-3)\times(3l-3)}$, and $\mathbf{Z} \in \mathbb{R}^{(3l-3)\times(3l-3)}$, were constructed by the authors in order to vectorize the recursive formula, and they are defined as follows:

$$\mathbf{X} = \begin{bmatrix} M_{x_{3\times 3}} & \cdots & 0_{3\times 3} & \cdots & 0_{3\times 3} \\ \vdots & \ddots & \vdots & \ddots & \vdots \\ 0_{3\times 3} & \cdots & M_{x_{3\times 3}} & \cdots & 0_{3\times 3} \\ \vdots & \ddots & \vdots & \ddots & \vdots \\ 0_{3\times 3} & \cdots & 0_{3\times 3} & \cdots & M_{x_{3\times 3}} \end{bmatrix},\ \mathbf{Y} = \begin{bmatrix} M_{y_{3\times 3}} & \cdots & 0_{3\times 3} & \cdots & 0_{3\times 3} \\ \vdots & \ddots & \vdots & \ddots & \vdots \\ 0_{3\times 3} & \cdots & M_{y_{3\times 3}} & \cdots & 0_{3\times 3} \\ \vdots & \ddots & \vdots & \ddots & \vdots \\ 0_{3\times 3} & \cdots & 0_{3\times 3} & \cdots & M_{y_{3\times 3}} \end{bmatrix},$$

$$\mathbf{Z} = \begin{bmatrix} M_{z_{3\times 3}} & \cdots & 0_{3\times 3} & \cdots & 0_{3\times 3} \\ \vdots & \ddots & \vdots & \ddots & \vdots \\ 0_{3\times 3} & \cdots & M_{z_{3\times 3}} & \cdots & 0_{3\times 3} \\ \vdots & \ddots & \vdots & \ddots & \vdots \\ 0_{3\times 3} & \cdots & 0_{3\times 3} & \cdots & M_{z_{3\times 3}} \end{bmatrix}$$

Now, the following approximation for the demanded current i_d^{pon} is found:

$$i_d^{pon} = \begin{bmatrix} 2\,\mathrm{diag}^{-1}\left(\mathbf{X}V_d^{pon,t}\right)P_d^p - \mathrm{diag}^{-2}\left(\mathbf{X}V_d^{pon,t}\right)\mathrm{diag}\left(P_d^p\right)\mathbf{X}V_d^{pon,t+1} + \\ 2\,\mathrm{diag}^{-1}\left(\mathbf{Y}V_d^{pon,t}\right)P_d^n - \mathrm{diag}^{-2}\left(\mathbf{Y}V_d^{pon,t}\right)\mathrm{diag}\left(P_d^n\right)\mathbf{Y}V_d^{pon,t+1} + \\ 2\,\mathrm{diag}^{-1}\left(\mathbf{Z}V_d^{pon,t}\right)P_d^{p-n} - \mathrm{diag}^{-2}\left(\mathbf{Z}V_d^{pon,t}\right)\mathrm{diag}\left(P_d^{p-n}\right)\mathbf{Z}V_d^{pon,t+1} \end{bmatrix} \tag{24}$$

With the approximation of the currents in Equation (24), it is possible to reach a general formula for bipolar DC grids by combining it with Equation (21), as presented in Equation (25).

$$V_d^{pon,t+1} = -\left[G_{\exp}^{pon}\left(V_d^{pon,t}\right)\right]^{-1}\begin{bmatrix} G_{ds}^{pon}V_s^{pon} + 2\,\mathrm{diag}^{-1}\left(\mathbf{X}V_d^{pon,t}\right)P_d^p + \\ 2\,\mathrm{diag}^{-1}\left(\mathbf{Y}V_d^{pon,t}\right)P_d^n + 2\,\mathrm{diag}^{-1}\left(\mathbf{Z}V_d^{pon,t}\right)P_d^{p-n} \end{bmatrix}, \tag{25}$$

where

$$G_{\exp}^{pon}\left(V_d^{pon,t}\right) = \begin{bmatrix} G_{dd}^{pon} - \mathrm{diag}^{-2}\left(\mathbf{X}V_d^{pon,t}\right)\mathrm{diag}\left(P_d^p\right)\mathbf{X} - \\ \mathrm{diag}^{-2}\left(\mathbf{Y}V_d^{pon,t}\right)\mathrm{diag}\left(P_d^n\right)\mathbf{Y} - \\ \mathrm{diag}^{-2}\left(\mathbf{Z}V_d^{pon,t}\right)\mathrm{diag}\left(P_d^{p-n}\right)\mathbf{Z} \end{bmatrix}$$

Note that the recursive power flow Formula (25) is evaluated from the initial point $t = 0$ by assigning the voltage at each node that is equal to the substation bus until the convergence criterion is met, i.e.,

$$\max\left\{\left\|\,|V_d^{pon,t+1}| - |V_d^{pon,t}|\,\right\|\right\} \leq \varepsilon. \tag{26}$$

3. Test Feeders

This section presents three bipolar DC grids that were used in the numerical validations of the proposed hyperbolic power flow approximation. These systems were composed of 4, 21, and 85 buses. All of the information of these test feeders is presented below.

3.1. The Four-Bus System

The four-bus system is a radial bipolar DC network composed of four nodes and three lines; the slack bus is located at node 1, and it is operated at ±220 V in the positive and negative poles and at 0 V in the neutral pole. The demand information per pole in this system is presented in Table 1,

Table 1. Branch and load parameters for the four-bus grid.

Node j	Node k	R_{jk} (Ω)	P_{dk}^p (W)	P_{dk}^n (W)	P_{dk}^{p-n} (W)
1	2	0.25	500	700	950
2	3	0.50	750	350	0
3	4	0.45	250	600	700

3.2. The 21-Bus System

The 21-bus grid is an adaptation of the monopolar DC network reported in [26]. The electrical configuration of this network is presented in Figure 3.

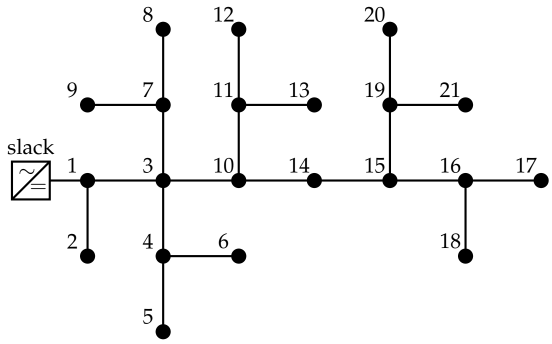

Figure 3. Grid configuration of the 21-bus system.

The 21-bus grid has a radial configuration with a voltage output in the slack node of ±1 kV and with 0 V in the neutral point. The complete parametric information for this test feeder is listed in Table 2.

Table 2. Parametric information of the 21-bus system (all powers are in kW).

Node j	Node k	R_{jk} (Ω)	P_{dk}^{p}	P_{dk}^{n}	P_{dk}^{p-n}
1	2	0.053	70	100	0
1	3	0.054	0	0	0
3	4	0.054	36	40	120
4	5	0.063	4	0	0
4	6	0.051	36	0	0
3	7	0.037	0	0	0
7	8	0.079	32	50	0
7	9	0.072	80	0	100
3	10	0.053	0	10	0
10	11	0.038	45	30	0
11	12	0.079	68	70	0
11	13	0.078	10	0	75
10	14	0.083	0	0	0
14	15	0.065	22	30	0
15	16	0.064	23	10	0
16	17	0.074	43	0	60
16	18	0.081	34	60	0
14	19	0.078	9	15	0
19	20	0.084	21	10	50
19	21	0.082	21	20	0

3.3. The 85-Bus System

This 85-bus grid with bipolar configuration corresponds to an adaptation of the IEEE 85-bus grid presented in [31]. For this test feeder, the substation bus is located at node 1 with a voltage output of ±11 kV for the positive and negative poles and 0 V in the neutral point. The electrical configuration of the 85-bus grid is depicted in Figure 4.

Information regarding the branch and load parameters for this test feeder is reported in Table 3.

Table 3. Data of the 85-bus system (all powers are in kW).

Node j	Node k	R_{jk} (Ω)	P_{dk}^{p}	P_{dk}^{p}	P_{dk}^{p-n}
1	2	0.108	0	0	10.075
2	3	0.163	50	0	40.35
3	4	0.217	28	28.565	0
4	5	0.108	100	50	0
5	6	0.435	17.64	17.995	25.18
6	7	0.272	0	8.625	0
7	8	1.197	17.64	17.995	30.29
8	9	0.108	17.8	350	40.46
9	10	0.598	0	100	0
10	11	0.544	28	28.565	0
11	12	0.544	0	40	45
12	13	0.598	45	40	22.5
13	14	0.272	17.64	17.995	35.13
14	15	0.326	17.64	17.995	20.175
2	16	0.728	17.64	67.5	33.49
3	17	0.455	56.1	57.15	50.25
5	18	0.820	28	28.565	200
18	19	0.637	28	28.565	10
19	20	0.455	17.64	17.995	150
20	21	0.819	17.64	70	152.5
21	22	1.548	17.64	17.995	30
19	23	0.182	28	75	28.565
7	24	0.910	0	17.64	17.995
8	25	0.455	17.64	17.995	50
25	26	0.364	0	28	28.565
26	27	0.546	110	75	175
27	28	0.273	28	125	28.565
28	29	0.546	0	50	75
29	30	0.546	17.64	0	17.995
30	31	0.273	17.64	17.995	0
31	32	0.182	0	175	0
32	33	0.182	7	7.14	12.5
33	34	0.819	0	0	0
34	35	0.637	0	0	50
35	36	0.182	17.64	0	17.995
26	37	0.364	28	30	28.565
27	38	1.002	28	28.565	25
29	39	0.546	0	28	28.565
32	40	0.455	17.64	0	17.995
40	41	1.002	10	0	0
41	42	0.273	17.64	25	17.995
41	43	0.455	17.64	17.995	0
34	44	1.002	17.64	17.995	0
44	45	0.911	50	17.64	17.995
45	46	0.911	25	17.64	17.995
46	47	0.546	7	7.14	10
35	48	0.637	0	10	0
48	49	0.182	0	0	25
49	50	0.364	18.14	0	18.505
50	51	0.455	28	28.565	0
48	52	1.366	30	0	15
52	53	0.455	17.64	35	17.995

Table 3. *Cont.*

Node j	Node k	R_{jk} (Ω)	P_{dk}^{p}	P_{dk}^{p}	P_{dk}^{p-n}
53	54	0.546	28	30	28.565
52	55	0.546	38	0	48.565
49	56	0.546	7	40	32.14
9	57	0.273	48	35.065	10
57	58	0.819	0	50	0
58	59	0.182	18	28.565	25
58	60	0.546	28	43.565	0
60	61	0.728	18	28.565	30
61	62	1.002	12.5	29.065	0
60	63	0.182	7	7.14	5
63	64	0.728	0	0	50
64	65	0.182	12.5	25	37.5
65	66	0.182	40	48.565	33
64	67	0.455	0	0	0
67	68	0.910	0	0	0
68	69	1.092	13	18.565	25
69	70	0.455	0	20	0
70	71	0.546	17.64	38.275	17.995
67	72	0.182	28	13.565	0
68	73	1.184	30	0	0
73	74	0.273	28	50	28.565
73	75	1.002	17.64	6.23	17.995
70	76	0.546	38	48.565	0
65	77	0.091	7	17.14	25
10	78	0.637	28	6	28.565
67	79	0.546	17.64	42.995	0
12	80	0.728	28	28.565	30
80	81	0.364	45	0	75
81	82	0.091	28	53.75	0
81	83	1.092	12.64	32.995	62.5
83	84	1.002	62	72.2	0
13	85	0.819	10	10	10

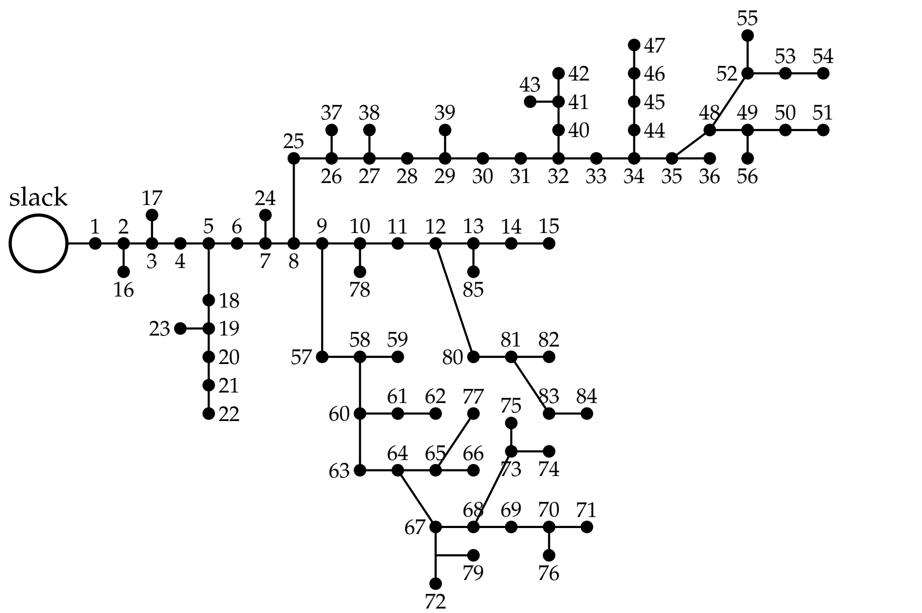

Figure 4. Grid topology of the IEEE 85-bus system for bipolar power flow applications.

4. Computational Validation

The implementation of the proposed hyperbolic approximation for the power flow solution in DC bipolar grids with multiple unbalanced loads was executed in MATLAB 2021*b* on a PC with an AMD Ryzen 7 3700 2.3-GHz processor and 16.0 GB of RAM, running on a 64-bit version of Microsoft Windows 10 Single Language. The methodology was compared to the successive approximation method proposed in [26] with its corresponding bipolar adaptation. Furthermore, the authors of these articles reported that successive approximation is completely equivalent to the classic backward/forward algorithm in the calculation of the power flow model.

4.1. Results in the Four-Bus Grid

For this test feeder, we considered two simulation cases, i.e., the neutral wire solidly grounded in all of the buses and the neutral wire grounded only at the substation bus. Table 4 presents the voltage in the positive, neutral, and negative poles. Both cases were solved with the proposed hyperbolic power flow approximation; Table 5 presents the solutions obtained with the successive approximation power flow method.

Table 4. Voltage profiles for both simulation cases with the proposed hyperbolic power flow approximation.

Node	+Pole (V)	0 Pole (V)	−Pole (V)
		Grounded neutral	
1	220	0	−220
2	217.2970	0	−217.1193
3	214.1348	0	−214.0633
4	212.8650	0	−212.0487
	Power losses	113.6987 W	
	Number of iterations	3	
		Non-grounded neutral	
1	220	0	−220
2	217.2990	−0.1834	−217.1155
3	214.1399	−0.0864	−214.0535
4	212.8721	−0.8384	−212.0337
	Power losses	115.2222 W	
	Number of iterations	3	

Table 5. Voltage profiles for both simulation cases with the successive approximation power flow method.

Node	+Pole (V)	0 Pole (V)	−Pole (V)
		Grounded neutral	
1	220	0	−220
2	217.2970	0	−217.1193
3	214.1348	0	−214.0633
4	212.8650	0	−212.0487
	Power losses	113.6987 W	
	Number of iterations	7	
		Non-grounded neutral	
1	220	0	−220
2	217.2990	−0.1834	−217.1155
3	214.1399	−0.0864	−214.0535
4	212.8721	−0.8384	−212.0337
	Power losses	115.2222 W	
	Number of iterations	8	

The numerical results in Table 5 show that: (i) The successive approximation power flow approach and the hyperbolic power flow proposal reached the same numerical voltages with a tolerance assigned to 1×10^{-10} and the same power losses for both simulation cases; however, the number of iterations of the hyperbolic approximation method was three for the solidly grounded case and eight for the non-solidly grounded scenario, while the successive approximation power flow method took seven iterations for the solidly grounded case and eight iterations for the non-grounded case. This behavior was attributed to the linear convergence of the successive approximation power flow method, while the hyperbolic approximation exhibited quadratic convergence, as demonstrated in [16]. (ii) As expected, the non-grounded neutral wire presented high power losses compared to those in the solidly grounded case. This situation occurred due to the currents that flowed through the neutral wire because of the presence of monopolar constant-power DC terminals. (iii) The voltage regulation for the solidly grounded neutral wire case was 3.6142%, and in the non-grounded scenario, it was 3.6210%. In addition, it was noted that, due to the load imbalances in the monopolar loads, the positive and negative voltage magnitudes per node differed among them.

4.2. Results in the 21-Bus Grid

Considering that the solution reached by the hyperbolic approximation took fewer iterations and ensured the same numerical results as those of the successive approximation power flow method with fewer iterations, here, we only present the results reached by our proposal. Table 6 presents the voltage profile performance for the 21-bus grid in the solidly grounded and non-grounded simulation scenarios.

Table 6. Voltages for both simulation cases in the 21-bus system.

Node	+Pole (V)	0 Pole (V)	−Pole (V)
		Grounded neutral	
1	1000	0	−1000
2	996.2761	0	−994.6716
3	960.0683	0	−968.4100
4	952.3714	0	−962.7830
5	952.1067	0	−962.7830
6	950.4396	0	−962.7830
7	953.7448	0	−964.5412
8	951.0867	0	−960.4284
9	943.8619	0	−960.7609
10	937.4888	0	−948.4698
11	930.9220	0	−942.8952
12	925.1152	0	−936.9933
13	926.9467	0	−939.7613
14	916.4715	0	−930.2940
15	905.4444	0	−921.0085
16	896.1420	0	−913.9505
17	890.1027	0	−911.4861
18	893.0582	0	−908.6017
19	909.9528	0	−924.3558
20	905.7061	0	−921.1448
21	908.0565	0	−922.5781
Power losses		91.2701 kW	
Number of iterations		4	

Table 6. *Cont.*

Node	+Pole (V)	0 Pole (V)	−Pole (V)
		Non-grounded neutral	
1	1000	0	−1000
2	996.2821	−1.6193	−994.6628
3	959.5205	9.2157	−968.7363
4	951.7636	11.3722	−963.1358
5	951.4955	11.6403	−963.1358
6	949.8030	13.3327	−963.1358
7	953.1183	11.7700	−964.8884
8	950.4291	10.3922	−960.8213
9	943.1110	17.9963	−961.1073
10	936.5746	12.4855	−949.0602
11	929.9259	13.6204	−943.5464
12	924.0247	13.7095	−937.7342
13	925.9357	14.4762	−940.4119
14	915.1628	15.9904	−931.1532
15	903.9040	18.1140	−922.0181
16	894.4081	20.6576	−915.0657
17	888.2594	24.3408	−912.6002
18	891.2522	18.5786	−909.8309
19	908.5513	16.7359	−925.2872
20	904.2616	17.8323	−922.0939
21	906.6158	16.9276	−923.5434
Power losses		95.4237 kW	
Number of iterations		4	

The numerical results in Table 6 show that: (i) The numbers of iterations with the hyperbolic approximation were four for the solidly grounded case and 13 for the non-grounded scenario, while the successive approximation power flow method took 10 iterations in the solidly grounded case and 13 in the non-grounded scenario. (ii) The effect of the neutral wire grounded in all of the nodes of the network was very positive in terms of the amount power loss, since for this scenario, this was 91.2701 kW, while in the non-grounded case, the power loss increased until 95.4237 kW, i.e., 4.2136 kW of additional losses. (iii) The voltage regulation when the neutral wire was solidly grounded was defined by the positive pole at node 17, since it had a low voltage profile with a magnitude of 890.1027 pu, which defined a regulation of 10.9897% for the 21-bus system in this simulation case. In addition, when the neutral wire was non-grounded, the minimum voltage was maintained at node 17 with a magnitude of 888.2594 V for the positive pole, which produced a regulation in the whole system of 11.1741%, which was worse than that in the solidly grounded case; however, this situation was explained by the additional voltage droops in the neutral wire due to the absence of the grounded system at each node. (iv) In the non-grounded neutral wire scenario, the voltage at this conductor reached about 24.3408 V at node 17; even though this is a low voltage value, it can cause the misoperation of electronic devices in areas near this node, since power electronic devices can be sensitive to variations in the voltage magnitudes of their local references.

To demonstrate the ability of the proposed hyperbolic approximation to deal with the power flow problem in meshed DC bipolar configurations, here, we add two lines to the 21-bus system that allow the radial configuration to become a meshed one. The added distribution lines connect node 7 with node 19 and node 11 with node 16, with resistances per pole of 0.082 and 0.037 Ω, respectively.

The numerical simulations of the meshed configuration for the 21-bus system showed that: (i) The total power losses in this system with a solidly grounded neutral wire were

75.1832 kW, while for the non-grounded scenario, these were 78.7372 kW, i.e., as expected, there was an increment in the power losses of 3.5540 kW due to the currents that flowed through the neutral conductor. (ii) The performances of the voltage profiles in both simulation cases were very similar, as can be seen in Figure 5; however, there were some differences when comparing the voltage magnitudes between the positive and negative poles. For the solidly grounded simulation case, the magnitude of the voltage at node 17 for the positive pole decreased until 0.9252 pu, while for the negative pole, the minimum voltage occurred at node 18 with a magnitude of 0.9392 pu. It is important to mention that these differences between poles for this particular neutral wire connection are attributable to the imbalances caused by monopolar loads due to the positive pole having a total monopolar load of 554 kW, while the total load in the negative pole was 445 kW.

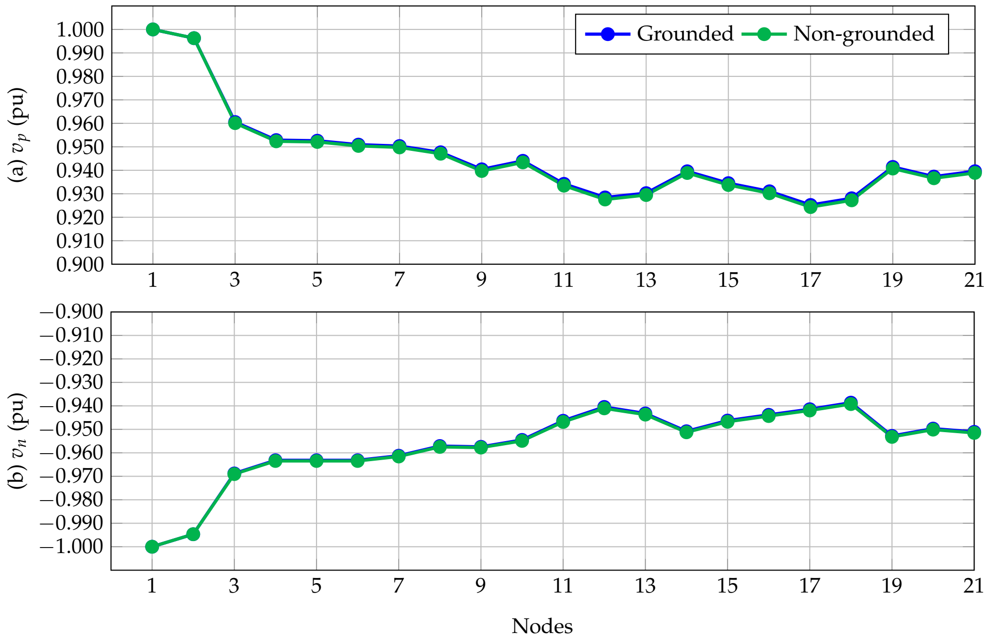

Figure 5. Behavior of the voltage profiles for the meshed configuration of the 21-bus system with the grounded and non-grounded connections of the neutral wire.

For the meshed configuration, the total number of iterations of the proposed hyperbolic approximation method was four in both simulation cases; the successive approximation method took nine iterations in the solidly grounded case and 11 in the non-grounded neutral wire simulation scenario.

4.3. Results in the 85-Bus Grid

When the proposed hyperbolic power flow approximation was applied to the 85-bus system, the following results were obtained: (i) When the neutral wire was solidly grounded, the total power losses for this system were 452.2981 kW, i.e., 6.76% of the total power consumption; however, when the neutral wire was non-grounded, these power losses increased to 489.5759 kW, i.e., 7.32% of the net power consumption. Hence, there was an additional 37.2778 kW of power losses. (ii) The total numbers of iterations were about four for the solidly grounded case and 13 for the non-grounded case.

The voltage profiles in the 85-bus system for the positive and negative poles considering the solidly grounded and non-grounded operation cases are presented in Figure 6.

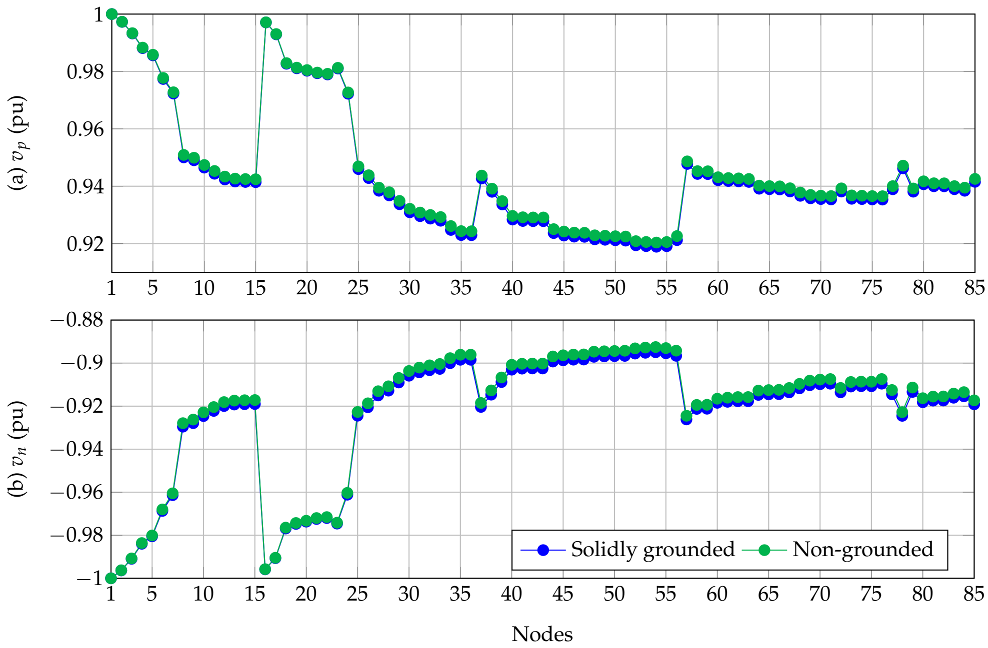

Figure 6. Voltage behavior for the 85-bus grid considering a solidly grounded or non-grounded neutral wire.

The voltage profiles in Figure 6 show that: (i) For the solidly grounded case, the operative costs of the minimum voltage in the positive pole were 0.9189 pu at node 54, and for the negative pole, they were 0.8950 pu at the same node. (ii) In the non-grounded scenario, these values were 0.9204 pu for the positive pole and 0.8925 pu for the negative pole.

Note that when the positive and negative voltage profiles are compared (see Figure 6a,b), it can be observed that the positive pole had a similar behavior to that of the negative pole, which was very similar to the reflection of the voltage profile with respect to the axis of the nodes; even if the system were to be perfectly balanced, then v_p must be equal to the absolute value of v_n.

4.4. Simulations Using the Quasi-Newton Formulation

To demonstrate the effectiveness of the proposed bipolar power flow formulation based on the hyperbolic approximation of the relation between the voltage and power relations in the power balance equation, here, we use an approximated solution method known as the quasi-Newton approach, which consists of calculating the Jacobian matrix only one time and keeping it constant during the entire iteration process. To implement the quasi-Newton method, the power flow Formulas (15) and (26) take the following structures:

$$V_d^{pn,t+1} = -\left[G_{\exp}^{pn}\left(V_d^{pn,0}\right)\right]^{-1}\begin{bmatrix} G_{ds}^{pn}V_s^{pn} + 2\,\mathrm{diag}^{-1}\left(V_d^{pn,t}\right)P_d^{pn} - \\ 2\,\mathrm{diag}^{-1}\left((\mathbf{J}-\mathbf{M})V_d^{pn,t}\right)P_d^{pn-np} \end{bmatrix}, \tag{27}$$

where

$$G_{\exp}^{pn}\left(V_d^{pn,0}\right) = \begin{bmatrix} G_{dd}^{pn} - \mathrm{diag}^{-2}\left(V_d^{pn,0}\right)\mathrm{diag}\left(P_d^{pn}\right) - \\ \mathrm{diag}^{-2}\left((\mathbf{J}-\mathbf{M})V_d^{pn,0}\right)\mathrm{diag}\left(P_d^{pn-np}\right)(\mathbf{J}-\mathbf{M}) \end{bmatrix}$$

and,

$$V_d^{pon,t+1} = -\left[G_{\exp}^{pon}\left(V_d^{pon,0}\right)\right]^{-1}\begin{bmatrix} G_{ds}^{pon}V_s^{pon} + 2\,\mathrm{diag}^{-1}\left(\mathbf{X}V_d^{pon,t}\right)P_d^{p} + \\ 2\,\mathrm{diag}^{-1}\left(\mathbf{Y}V_d^{pon,t}\right)P_d^{n} + 2\,\mathrm{diag}^{-1}\left(\mathbf{Z}V_d^{pon,t}\right)P_d^{p-n} \end{bmatrix}, \tag{28}$$

where

$$G_{\exp}^{pon}\left(V_d^{pon,0}\right) = \begin{bmatrix} G_{dd}^{pon} - \text{diag}^{-2}\left(\mathbf{X}V_d^{pon,0}\right)\text{diag}\left(P_d^p\right)\mathbf{X}- \\ \text{diag}^{-2}\left(\mathbf{Y}V_d^{pon,0}\right)\text{diag}\left(P_d^n\right)\mathbf{Y}- \\ \text{diag}^{-2}\left(\mathbf{Z}V_d^{pon,0}\right)\text{diag}\left(P_d^{p-n}\right)\mathbf{Z} \end{bmatrix}$$

The main advantage of keeping the Jacobian matrix constant for the solidly and non-solidly grounded cases corresponds to the possibility of calculating it and storing it to be used in the recursive power flow formula without making inversions each time, which makes the processing times required to solve the power flow problem minor in comparison with the time taken by the original power flow formulation. One of the main advantages of keeping the Jacobian matrix constant for the cases studied here (solidly and non-solidly grounded cases) corresponds to the possibility of calculating it one time and storing it as a constant in order to be used in the recursive power flow formula without making inversions at each iteration; this approach reduces the processing times required to solve the power flow problem, but it increases the number of iterations required for the convergence of the algorithm.

5. Conclusions

A power flow model based on the Taylor expansion of the hyperbolic equation of the bus injection model in bipolar DC networks was addressed in this work. This formulation applies to radial and meshed grids. The method was compared to the well-known successive approximation algorithm, demonstrating fast convergence in terms of numbers of iterations and leading to the same point of operation (with an error of 1×10^{-10}); furthermore, the analysis of three benchmarks allowed a conclusion as to the scalability of our proposal, since it applies to systems with different numbers of nodes with reasonable execution times (and a low number of iterations). The numerical results demonstrated that it is desired to have a neutral wire that is solidly grounded in all the nodes, since the losses (and voltage imbalances) increase considerably due to the current in the neutral pole. However, this would be very expensive and impractical in real-life situations. Finally, it is essential to remark that the power flow is the basis for the development of algorithms and the study of other subjects, such as planning (which refers to studies such as the reconfiguration and expansion of a grid, the optimal selection, integration, and placement of distributed energy resources such as photovoltaic units or batteries, and other studies in the long term), operation (which is related to the optimal control of a grid), and protection (which is related to keeping a grid safe when there is a large disturbance on it) of bipolar DC networks.

In future work, it will be possible to develop the following: (i) the proposal of a sequential quadratic optimal power flow for bipolar DC grids with unbalanced loads based on the hyperbolic approximation presented in this research; (ii) the development of a mixed-integer conic formulation for solving the optimal pole-swapping problem in unbalanced bipolar DC networks; (iii) the practical implementation of a bipolar DC grid in order to test the proposed methodology for the power flow calculation; (iv) the detailed exploration of the effect of a non-solidly grounded neutral wire in the expected convergence of the proposed hyperbolic power flow formulation regarding the large variations in the number of iterations with respect to the solidly grounded scenario for the neutral wire.

Author Contributions: Conceptualization, methodology, software, and writing (review and editing): S.S.-G., O.D.M. and A.G. All authors have read and agreed to the published version of the manuscript.

Funding: This research received no external funding.

Institutional Review Board Statement: Not applicable.

Informed Consent Statement: Not applicable.

Data Availability Statement: The data used in this study are reported in the paper's figures and tables.

Conflicts of Interest: The authors declare no conflict of interest.

References

1. Lotfi, H.; Khodaei, A. AC Versus DC Microgrid Planning. *IEEE Trans. Smart Grid* **2017**, *8*, 296–304. [CrossRef]
2. Barros, J.; de Apráiz, M.; Diego, R. Power Quality in DC Distribution Networks. *Energies* **2019**, *12*, 848. [CrossRef]
3. Elsayed, A.T.; Mohamed, A.A.; Mohammed, O.A. DC microgrids and distribution systems: An overview. *Electr. Power Syst. Res.* **2015**, *119*, 407–417. [CrossRef]
4. Mackay, L.; van der Blij, N.H.; Ramirez-Elizondo, L.; Bauer, P. Toward the Universal DC Distribution System. *Electr. Power Components Syst.* **2017**, *45*, 1032–1042. [CrossRef]
5. Kumar, J.; Agarwal, A.; Agarwal, V. A review on overall control of DC microgrids. *J. Energy Storage* **2019**, *21*, 113–138. [CrossRef]
6. Parhizi, S.; Lotfi, H.; Khodaei, A.; Bahramirad, S. State of the Art in Research on Microgrids: A Review. *IEEE Access* **2015**, *3*, 890–925. [CrossRef]
7. Chauhan, R.K.; Rajpurohit, B.S.; Pindoriya, N.M. DC Power Distribution System for Rural Applications. In Proceedings of the 8th National Conference on Indian Energy Sector Synergy with Energy, Ahmadabad, India, 11–12 October 2012. [CrossRef]
8. Justo, J.J.; Mwasilu, F.; Lee, J.; Jung, J.W. AC-microgrids versus DC-microgrids with distributed energy resources: A review. *Renew. Sustain. Energy Rev.* **2013**, *24*, 387–405. [CrossRef]
9. Kalair, A.; Abas, N.; Khan, N. Comparative study of HVAC and HVDC transmission systems. *Renew. Sustain. Energy Rev.* **2016**, *59*, 1653–1675. [CrossRef]
10. Dastgeer, F.; Gelani, H.E. A Comparative analysis of system efficiency for AC and DC residential power distribution paradigms. *Energy Build.* **2017**, *138*, 648–654. [CrossRef]
11. Vossos, V.; Garbesi, K.; Shen, H. Energy savings from direct-DC in U.S. residential buildings. *Energy Build.* **2014**, *68*, 223–231. [CrossRef]
12. Kakigano, H.; Miura, Y.; Ise, T. Low-Voltage Bipolar-Type DC Microgrid for Super High Quality Distribution. *IEEE Trans. Power Electron.* **2010**, *25*, 3066–3075. [CrossRef]
13. Rivera, S.; Lizana, R.; Kouro, S.; Dragičević, T.; Wu, B. Bipolar DC Power Conversion: State-of-the-Art and Emerging Technologies. *IEEE J. Emerg. Sel. Top. Power Electron.* **2021**, *9*, 1192–1204. [CrossRef]
14. Tavakoli, S.D.; Mahdavyfakhr, M.; Hamzeh, M.; Sheshyekani, K.; Afjei, E. A unified control strategy for power sharing and voltage balancing in bipolar DC microgrids. *Sustain. Energy Grids Netw.* **2017**, *11*, 58–68. [CrossRef]
15. Gwon, G.H.; Kim, C.H.; Oh, Y.S.; Noh, C.H.; Jung, T.H.; Han, J. Mitigation of voltage unbalance by using static load transfer switch in bipolar low voltage DC distribution system. *Int. J. Electr. Power Energy Syst.* **2017**, *90*, 158–167. [CrossRef]
16. Montoya, O.D.; Gil-González, W.; Garces, A. Numerical methods for power flow analysis in DC networks: State of the art, methods and challenges. *Int. J. Electr. Power Energy Syst.* **2020**, *123*, 106299. [CrossRef]
17. Mishra, M.; Patnaik, B.; Biswal, M.; Hasan, S.; Bansal, R.C. A systematic review on DC-microgrid protection and grounding techniques: Issues, challenges and future perspective. *Appl. Energy* **2022**, *313*, 118810. [CrossRef]
18. Mandal, S.; Pahwa, A. Optimal Selection of Conductors for Distribution Feeders. *IEEE Power Eng. Rev.* **2002**, *22*, 71. [CrossRef]
19. Wang, P.; Wang, W.; Xu, D. Optimal Sizing of Distributed Generations in DC Microgrids With Comprehensive Consideration of System Operation Modes and Operation Targets. *IEEE Access* **2018**, *6*, 31129–31140. [CrossRef]
20. Altun, T.; Madani, R.; Yadav, A.P.; Nasir, A.; Davoudi, A. Optimal Reconfiguration of DC Networks. *IEEE Trans. Power Syst.* **2020**, *35*, 4272–4284. [CrossRef]
21. Meng, L.; Luna, A.; Diaz, E.; Sun, B.; Dragicevic, T.; Savaghebi, M.; Vasquez, J.; Guerrero, J.; Graells, M. Flexible System Integration and Advanced Hierarchical Control Architectures in the Microgrid Research Laboratory of Aalborg University. *IEEE Trans. Ind. Appl.* **2015**, *52*, 1736–1749. [CrossRef]
22. Roncero-Clemente, C.; Gonzalez-Romera, E.; Barrero-Gonzalez, F.; Milanes-Montero, M.I.; Romero-Cadaval, E. Power-Flow-Based Secondary Control for Autonomous Droop-Controlled AC Nanogrids With Peer-to-Peer Energy Trading. *IEEE Access* **2021**, *9*, 22339–22350. [CrossRef]
23. Abdi, H.; Beigvand, S.D.; Scala, M.L. A review of optimal power flow studies applied to smart grids and microgrids. *Renew. Sustain. Energy Rev.* **2017**, *71*, 742–766. [CrossRef]
24. Li, J.; Liu, F.; Wang, Z.; Low, S.H.; Mei, S. Optimal Power Flow in Stand-Alone DC Microgrids. *IEEE Trans. Power Syst.* **2018**, *33*, 5496–5506. [CrossRef]
25. Grisales-Noreña, L.F.; Montoya, O.D.; Gil-González, W.J.; Perea-Moreno, A.J.; Perea-Moreno, M.A. A Comparative Study on Power Flow Methods for Direct-Current Networks Considering Processing Time and Numerical Convergence Errors. *Electronics* **2020**, *9*, 2062. [CrossRef]
26. Medina-Quesada, A.; Montoya, O.D.; Hernández, J.C. Derivative-Free Power Flow Solution for Bipolar DC Networks with Multiple Constant Power Terminals. *Sensors* **2022**, *22*, 2914. [CrossRef]
27. Lee, J.O.; Kim, Y.S.; Jeon, J.H. Generic power flow algorithm for bipolar DC microgrids based on Newton–Raphson method. *Int. J. Electr. Power Energy Syst.* **2022**, *142*, 108357. [CrossRef]

28. Lee, J.O.; Kim, Y.S.; Moon, S.I. Current Injection Power Flow Analysis and Optimal Generation Dispatch for Bipolar DC Microgrids. *IEEE Trans. Smart Grid* **2021**, *12*, 1918–1928. [CrossRef]
29. Mackay, L.; Guarnotta, R.; Dimou, A.; Morales-Espana, G.; Ramirez-Elizondo, L.; Bauer, P. Optimal Power Flow for Unbalanced Bipolar DC Distribution Grids. *IEEE Access* **2018**, *6*, 5199–5207. [CrossRef]
30. Chew, B.S.H.; Xu, Y.; Wu, Q. Voltage Balancing for Bipolar DC Distribution Grids: A Power Flow Based Binary Integer Multi-Objective Optimization Approach. *IEEE Trans. Power Syst.* **2019**, *34*, 28–39. [CrossRef]
31. Tamilselvan, V.; Jayabarathi, T.; Raghunathan, T.; Yang, X.S. Optimal capacitor placement in radial distribution systems using flower pollination algorithm. *Alex. Eng. J.* **2018**, *57*, 2775–2786. [CrossRef]